J. Fluid Mech. (1992), *vol.* 241, *pp.* 421–442
Printed in Great Britain

Parallel flow in Hele-Shaw cells

By M. ZEYBEK AND Y. C. YORTSOS†
Petroleum Engineering Program, Department of Chemical Engineering, University of Southern California, Los Angeles, CA 90089-1211, USA

(Received 19 July 1991 and in revised form 20 December 1991)

We consider the parallel flow of two immiscible fluids in a Hele-Shaw cell. The evolution of disturbances on the fluid interfaces is studied both theoretically and experimentally in the large-capillary-number limit. It is shown that such interfaces support wave motion, the amplitude of which for long waves is governed by a set of KdV and Airy equations. The waves are dispersive provided that the fluids have unequal viscosities and that the space occupied by the inner fluid does not pertain to the Saffman–Taylor conditions (symmetric interfaces with half-width spacing). Experiments conducted in a long and narrow Hele-Shaw cell appear to validate the theory in both the symmetric and the non-symmetric cases.

1. Introduction

During the past several years the flow of immiscible fluids in Hele-Shaw cells and porous media has been investigated extensively. Of particular interest to most studies has been frontal displacement, specifically viscous fingering instabilities and finger growth. This can be readily understood in view of the many interesting theoretical and practical problems associated with such fronts. For Hele-Shaw cells, we mention the selection problems and the singular perturbation associated with the high-capillary-number limit (Bensimon *et al.* 1986; Combescot *et al.* 1986), and the relation of viscous fingers to crystal growth (Pelcé 1988) and flame front dynamics (Zel'dovich *et al.* 1980). In porous media, unstable frontal displacement has been highlighted with the use of diffusion-limited-aggregation (Witten & Sanders 1981) and other probabilistic growth models (King 1987). Issues of capillarity, heterogeneity, randomness and spatial correlation, including fractal statistics (Emanuel *et al.* 1989; Lenormand 1989; Lenormand *et al.* 1990; Lenormand, Touboul & Zarcone 1988), have been extensively explored, although several questions still remain unanswered (Yortsos 1990). The practical ramifications regarding oil recovery, as well as many other industrial processes in porous media, have served as the primary driving force for most of these investigations.

By contrast, little attention has been paid to the motion of lateral fluid interfaces, which are parallel to the main flow direction. Parallel flow is an often encountered, although much overlooked regime. In the context of Hele-Shaw displacement, it is the theoretical limit of fully developed fingers (e.g. the Saffman–Taylor (1958) finger) (see figure 1). Parallel flow conditions have been invoked in qualitative support of the scaling properties of unstable non-capillary displacement in porous media. Concerning the latter, it has been shown (King & Sher 1990; Lee, Coniglio & Stanley 1990) that as long as the viscosity ratio M is finite, the initially fractal displacing fluid

† To whom correspondence should be addressed.

cluster eventually evolves into a compact Euclidean object (although its perimeter may be a self-affine fractal (King & Sher 1990; King 1987; Lee *et al.* 1990)). In a different context, parallel flow is often realized in thin and long reservoirs, typically masked under the assumption of vertical flow equilibrium (Coats, Dempsey & Anderson 1971; Yokayama & Lake 1981; Zapata & Lake 1981). Recent studies on viscous fingering in porous media have invoked parallel flow to develop approximate models that satisfy numerical experiments (Fayers 1988; Fayers & Newley 1988). Finally, we mention that parallel flow is routinely encountered in yet other contexts, for example the steady-state, concurrent flow in relative permeability measurements (Collins 1967), as well as in processes involving counter-current imbibition (Kalaydjian & Legait 1987). Although not directly relevant to this work, the pore-level analysis of such flows is very incomplete at present, despite recent advances in the understanding of viscous coupling between phases (Aul & Olbricht 1990) and efforts to ascribe a viscosity ratio dependence on steady-state relative permeabilities (Rothman 1990).

It is well known that, under the typical conditions of low $Re = \rho q b/\mu$ (where b denotes cell spacing), the flow of a single phase in Hele-Shaw cells and porous media (and more generally, multi-phase, multi-component flow, but in the absence of spatial and concentration gradients) is potential. Such purely viscous flow exists on either side of the interface between immiscible fluids in a Hele-Shaw cell (figure 1), and sufficiently far from the interface region in the case of porous media. We recall that potential flow (although in the opposite, inviscid limit) also governs the fluid flow in water waves (Lighthill 1987). We surmise that the dynamics of the lateral interfaces in parallel flow are likely to be related to those of shallow water waves (Hammack, Scheffner & Segur 1989).

It is with this idea in mind that we examine the dynamics of fluid interfaces in parallel flow in Hele-Shaw cells. In particular, the possibility of sustained wave propagation and the existence of solitons form the main subject of this paper. We present both theoretical and experimental evidence that, subject to certain conditions, supports the existence of dispersive waves in the parallel flow of two immiscible fluids. In the theoretical part, we first proceed with a linear analysis, which shows that small disturbances are dispersive, if the viscosity ratio M is not unity and the spacing of the 'inner' fluid does not correspond to the Saffman–Taylor finger configuration. Subsequently, a weakly nonlinear analysis is presented for long-wave, small-amplitude disturbances. The asymptotic description of the general problem is ultimately formulated in terms of a set of KdV and Airy equations. The solution of the former is obtained numerically, although analytical results are also used for comparison purposes. A brief summary of this work was given in Zeybek & Yortsos (1991). This paper presents a more detailed account, as well as the extension to the more general (non-symmetric) case.

We must point out that although there are many similarities with shallow water waves, there are also many differences. First, the use of two immiscible liquids in a Hele-Shaw cell invariably raises issues of wettability and capillarity. The latter acts to dissipate high-frequency waves, while under certain conditions the former may completely dominate the process. Such issues do not arise in shallow water waves, where it is viscous dissipation that results in an amplitude decrease. Secondly, for flat steady-state interfaces to develop between the two immiscible fluids, a parallel flow condition ($q_a \mu_a = q_b \mu_b$) at high values of the modified capillary number, N'_{ca}, must be first met. This requires a somewhat elaborate experimental procedure. Finally, solitary waves in shallow water wave experiments are typically detected by special

probes owing to their very small amplitude. Hele-Shaws cells make difficult the use of such probes. Therefore, the experiments were restricted to simple flow visualization.

To test the theoretical predictions, several experiments were conducted. First, we considered a configuration of two fluids separated by one interface. For reasons that will become apparent, we refer to this as the symmetric case. This configuration allows us to test and improve our experimental technique, and also to compare with well-known analytical results. After satisfactory results were obtained, experiments were carried out for the non-symmetric case, where two interfaces are involved. In all experiments, we attempted to generate single solitons on both interfaces as well as to seek the interaction of solitons. Compared to frontal displacement in Hele-Shaw experiments, the experiments are well reproduced. Flat interfaces are readily recovered, after the disturbance leaves the cell, and experimental runs can be easily reproduced. We should point out that in our experiments, the viscosity ratio was finite, contrary to most Hele-Shaw experiments reported in the literature, which are carried out at large viscosity ratio.

2. Theory

We examine the lateral interfaces between two immiscible and incompressible fluids of different viscosities in the parallel Hele-Shaw flow shown schematically in figure 1. The cell is horizontal and has half-width W. Parallel flow requires flat interfaces and the absence of pressure gradients in the transverse (Y) direction. This condition is satisfied by the requirement $\mu_b q_b = \mu_a q_a \equiv Q$, where μ_i denotes viscosity and q_i the flow velocity of fluid i. Under the above, steady-state interfaces are flat. We denote the normalized interface positions by λ_1 and λ_2 ($-1 \leqslant \lambda_2 \leqslant \lambda_1 \leqslant 1$), where transverse lengths are scaled with the half-width W. The basic governing equations follow from the usual Hele-Shaw assumptions. In each fluid, Darcy's law applies and the pressure satisfies the Laplace equation

$$\nabla^2 P_i = 0 \Rightarrow \nabla^2 \Phi_i = 0; \quad i = a, b. \tag{1}$$

Here, subscript a denotes the 'inner' fluid. Note that fluid b flows in two different, separated regions, thus two different pressures are needed for a full description. We describe the interfaces in dimensional notation by

$$\mathscr{F}_i(X, Y, T) \equiv Y - F_i(X, T) = 0; \quad i = 1, 2. \tag{2}$$

On each interface, the usual kinematic conditions apply, that fluid velocities normal to the interfaces are equal to each other and to the normal velocity of the interface itself

$$\boldsymbol{U}_b \cdot \boldsymbol{n}_i = \boldsymbol{U}_a \cdot \boldsymbol{n}_i; \quad i = 1, 2, \tag{3}$$

$$\boldsymbol{U}_a \cdot \boldsymbol{n}_i = -\frac{\mathscr{F}_{iT}}{|\nabla \mathscr{F}_i|}; \quad i = 1, 2, \tag{4}$$

where $\boldsymbol{n}_i = \nabla \mathscr{F}_i / |\nabla \mathscr{F}_i|$ is the normal vector. With the use of Darcy's law the above transform into

$$\nabla P_b \cdot \nabla \mathscr{F}_i = M \nabla P_a \cdot \nabla \mathscr{F}_i; \quad i = 1, 2, \tag{5}$$

$$\boldsymbol{U}_a \cdot \nabla \mathscr{F}_i = -\frac{\partial \mathscr{F}_i}{\partial T}; \quad i = 1, 2. \tag{6}$$

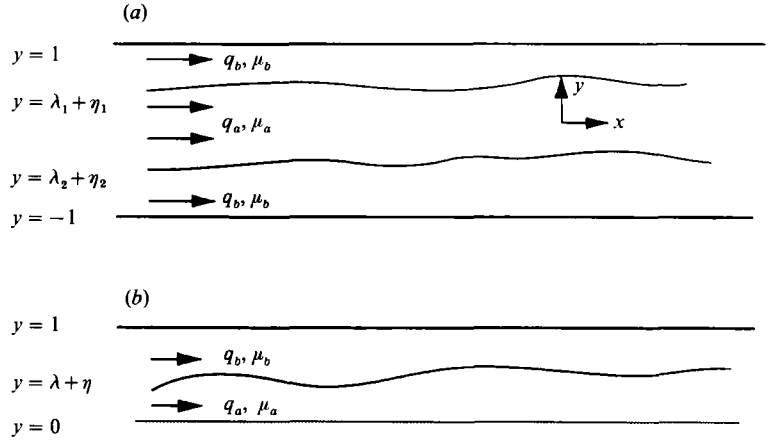

FIGURE 1. Flow geometry for (*a*) non-symmetric and (*b*) symmetric case.

Finally, across each interface the pressure drop is due to curvature, thus

$$\Delta P_j = \gamma \frac{F_{iXX}}{|\nabla \mathscr{F}_i|^3}; \quad j = a, b; \quad i = 1, 2, \tag{7}$$

where γ is the interfacial tension. Since the present interest is in long waves, higher-order corrections to pressure drop are of secondary importance. We point out briefly that this problem is different than the two problems studied by Park & Homsy (1984) for frontal displacement and by Burgess & Foster (1990) for flow at the side of a Hele-Shaw bubble, where capillarity dominates the leading-order approximations in the thin dimension. The present case requires a novel formulation, which is not considered here.

2.1. *Linear analysis*

The dynamics of flat interfaces parallel to the flow direction is next obtained by following an analysis in terms of normal modes. As a preliminary step, we investigate one interface only, corresponding to the symmetric problem $\lambda_1 = -\lambda_2, \eta_1 = -\eta_2$, where η_1 and η_2 describe the dimensionless disturbances of the two interfaces (see figure 1*b*). Using lower-case letters to denote dimensionless quantities, the dimensionless base interface is at location

$$\bar{f}_1 = \lambda_1, \tag{8}$$

while the base pressure satisfies

$$\bar{p}_i = -x; \quad i = a, b. \tag{9}$$

Here, we have scaled pressure by $q_a \mu_a L/k$, where $k = \frac{1}{12}b^2$ is the permeability of the Hele-Shaw cell, L is a streamwise length and time is scaled by L/q_a. The pressure and the interface are next perturbed as follows:

$$p_i = \bar{p}_i + p' = -x + \epsilon\, e^{i(\omega t - kx)} \phi_i(y); \quad i = a, b, \tag{10}$$

$$f_1 = \bar{f}_1 + B\epsilon\, e^{i(\omega t - kx)}. \tag{11}$$

After linearization and use of no-flow boundary conditions at $y = 1$ and $y = 0$, the following results for the potential disturbances are obtained:

$$\phi_b = K_1 \cosh(k(y-1)); \quad \lambda_1 < y < 1,$$

$$\phi_a = K_2 \cosh(ky); \quad 0 < y < \lambda_1.$$

Substitution into the interface conditions yields, after some algebra, the following result for the complex frequency ω:

$$\omega = 2\frac{k\sinh k}{(1+M)\sinh k+(1-M)\sinh k(1-2\lambda_1)} + \frac{\mathrm{i}}{6N'_{\mathrm{ca}}}\frac{2k^3\sinh(k\lambda_1)\sinh(k(1-\lambda_1))}{(1+M)\sinh k+(1-M)\sinh(k(1-2\lambda_1))}. \quad (12)$$

Here, $M \equiv \mu_b/\mu_a$ is defined as the ratio of the viscosity of the outer fluid b, to the viscosity of the inner fluid a (figure 1). We note that in the above relation, capillarity first enters at $O(k^4)$. Hence, for long waves (small k) and for a sufficiently large value of the modified capillary number, $N'_{\mathrm{ca}} = q_a\mu_a L^2/\gamma b^2$ (Homsy 1987), capillarity can be neglected, although it should be cautioned that three-dimensional effects may become important when the capillary number is too large (Maxworthy 1989). Under these conditions, the frequency is strictly real and the long-wave speed $c \equiv \omega/k$ can be expanded as

$$c = c_0\left[1-\frac{k^2}{3}\frac{(M-1)\lambda_1(1-2\lambda_1)(1-\lambda_1)}{1-\lambda_1+\lambda_1 M}+\ldots\right], \quad (13)$$

where $c_0 = 1/(1-\lambda_1+\lambda_1 M)$. For $M \neq 1$, the above relation predicts dispersive waves (Ablowitz & Segur 1981), i.e. waves with different wavelength travel with different speed. This result is quite different from the linear stability relations of frontal displacement, which yield either constant growth (viscous fingering) or constant decay. The existence of oscillatory modes in Hele-Shaw displacements was first reported in Yortsos & Zeybek (1989) and it is also in agreement with recent remarks by Xu (1991) and by Meiburg (1991). As expected, the waves become non-dispersive when the fluids have equal viscosity ($M = 1$). Interestingly, non-dispersive waves are also predicted for the Saffman–Taylor conditions ($\lambda_1 = \frac{1}{2}$), although the latter have infinitesimal velocity when $M \gg 1$.

An analysis similar to the above gives the dispersion relation for the non-symmetric case, where now two interfaces are involved (figure 1*a*). As expected, the dispersion relation is substantially more complicated. The final result is

$$\tanh(k(1-\lambda_1))[\mathrm{e}^{-k\lambda_1}aD+\mathrm{e}^{k\lambda_1}aE]-aM\,\mathrm{e}^{-k\lambda_1}D-b\,\mathrm{e}^{-k\lambda_1}D+b\,\mathrm{e}^{k\lambda_1}E+aM\,\mathrm{e}^{k\lambda_1}E = 0, \quad (14)$$

where

$$D = \mathrm{e}^{k\lambda_2}[(d-b)\sinh(k(1+\lambda_2))-Md\cosh(k(1+\lambda_2))],$$

$$E = \mathrm{e}^{-k\lambda_2}[(b-d)\sinh(k(1+\lambda_2))-Md\cosh(\alpha(1+\lambda_2))],$$

$$a = \mathrm{i}[1-\omega/k], \quad b = \mathrm{i}[1-M], \quad d = \mathrm{i}[1-(\omega/k)M].$$

For our purposes, we shall consider only the asymptotic expansion at small wavenumbers, by taking $c = x_0+x_1k+x_2k^2+\ldots$. Two solutions arise:

$$c_m = x_{0,m}+x_{2,m}k^2+\ldots; \quad m = 1,2, \quad (15)$$

where

$$x_{0,1} = \frac{1}{M}, \quad x_{0,2} = \frac{2}{\Delta}, \quad x_{2,1} = \frac{(M-1)(\lambda_1-1)(\lambda_2+1)(\lambda_1-\lambda_2)}{M^2(2+\lambda_2-\lambda_1)},$$

$$x_{2,2} = \frac{4}{3}\frac{(M-1)}{\Delta^2}\frac{(\lambda_1-\lambda_2)(1+\lambda_2-\lambda_1)[(\lambda_2+1)^2+(\lambda_1-1)^2+(\lambda_2+1)(\lambda_1-1)]}{(2+\lambda_2-\lambda_1)},$$

and where we have defined $\Delta \equiv 2+(M-1)(\lambda_1-\lambda_2)$. The two roots correspond to the two different amplitude equations for the two interfaces. As in the symmetric case, the waves are dispersive as long as $M \neq 1$.

2.2. *Weakly nonlinear analysis*

The linear analysis is limited to the description of the onset of motion. The subsequent dynamics can be obtained by a nonlinear analysis that includes higher-order effects. In this section, the evolution of these dispersive waves is investigated.

We shall apply a perturbation analysis similar to that used for shallow water waves, valid for small amplitudes and long wavelengths. We consider the initial value formulation as described in Kevorkian & Cole (1980). First, two key dimensionless parameters are defined: $\delta \equiv W/L$, where L is the initial length of the disturbance, and $\epsilon \equiv A/W$, where A is a measure of the initial disturbance amplitude. In this notation, the Laplace equation in each flow region is

$$\delta^2\phi_{ixx}+\phi_{iyy}=0; \quad i=a,1,2. \tag{16}$$

In the above, we have used subscripts 1 and 2 to denote the velocity potential of fluid b in the upper and lower regions, respectively. Correspondingly, the interface positions are at $y_i=\lambda_i+\eta_i\,(i=1,2)$. The interface conditions now read

$$\delta^2(\phi_{ix}-1)\,\eta_{ix}-\phi_{iy}=\delta^2M(\phi_{ax}-1)\,\eta_{ix}-M\phi_{ay}; \quad i=1,2, \tag{17}$$

$$\delta^2(\eta_{it}-\eta_{ix}(\phi_{ax}-1))=-\phi_{ay}; \quad i=1,2, \tag{18}$$

and in the absence of surface tension

$$\phi_a=\phi_i; \quad i=1,2.$$

The problem is fully specified with the no-flow boundary conditions at the sidewalls

$$\frac{\partial\phi_1}{\partial y}=0 \quad \text{at} \quad y=1,$$

$$\frac{\partial\phi_2}{\partial y}=0 \quad \text{at} \quad y=-1,$$

a sufficiently fast far-field decay of the disturbances

$$\eta_i\to 0 \quad \text{at} \quad |x|\to\infty,$$

and the initial condition

$$\eta_i(x,0)=\epsilon h_i(x).$$

To implement an asymptotic approach, a long-wave, long-time and small-amplitude approximation is considered, $\delta \ll 1, \tilde{t}=\epsilon t, \epsilon \ll 1$. Then, the following asymptotic expansions are taken:

$$\phi_i=\epsilon\phi_{i0}+\epsilon\delta^2\phi_{i1}+\epsilon\delta^4\phi_{i2}+\ldots; \quad i=1,2, \tag{19}$$

$$\eta_i=\epsilon\eta_{i0}+\epsilon^2\eta_{i1}+\ldots; \quad i=1,2, \tag{20}$$

where the various terms of the expansion also depend on $\tilde{t}$, e.g. $\eta_i \equiv \eta_i(x,t,\tilde{t})$. For non-trivial results to be obtained, the relation $\delta=\kappa\epsilon^{\frac{1}{2}}$ is necessary, as can be readily

shown with the method of dominant balance (Kevorkian & Cole 1980). Use of this in (19)–(20) and substitution into the field equations and in the interfaces conditions (17)–(18) yield the following results. At the zeroth order

$$\boldsymbol{\eta}_{0,t}+\boldsymbol{A}\cdot\boldsymbol{\eta}_{0,x}=0, \tag{21}$$

where the matrix

$$\boldsymbol{A}=\begin{bmatrix} \dfrac{M+1-(M-1)\lambda_2}{M\Delta} & \dfrac{(M-1)(\lambda_1-1)}{M\Delta} \\ \dfrac{-(1+\lambda_2)(M-1)}{M\Delta} & \dfrac{M+1+(M-1)\lambda_1}{M\Delta} \end{bmatrix}$$

has eigenvalues $2/\Delta$ and $1/M$. This system is diagonalized if we introduce the variable

$$\boldsymbol{v}_0=-\boldsymbol{L}\cdot\boldsymbol{\eta}_0 \tag{22}$$

where $$\boldsymbol{L}=\frac{1}{(2-\lambda_1+\lambda_2)}\begin{bmatrix} -1 & 1 \\ 1+\lambda_2 & 1-\lambda_1 \end{bmatrix}.$$

The components of $\boldsymbol{v}_0=[v_{10},v_{20}]^{\mathrm{T}}$ can be expressed in terms of η_{i0}:

$$v_{10}\equiv U=\frac{\eta_{10}-\eta_{20}}{2-\lambda_1+\lambda_2},$$

$$v_{20}\equiv V=-\frac{(1+\lambda_2)\eta_{10}+(1-\lambda_1)\eta_{20}}{2-\lambda_1+\lambda_2}. \tag{23}$$

It follows that variable U is proportional to the net transverse displacement of fluid a. From (21) and (22) we obtain

$$\boldsymbol{v}_{0,t}+\boldsymbol{D}\cdot\boldsymbol{v}_{0,x}=0, \tag{24}$$

where $$\boldsymbol{D}=\boldsymbol{L}^{-1}\boldsymbol{A}\boldsymbol{L}=\begin{bmatrix} \dfrac{2}{\Delta} & 0 \\ 0 & \dfrac{1}{M} \end{bmatrix}.$$

The solution of the initial value problem (24) is

$$v_{10}=f_0(\sigma,\tilde{t}) \tag{25}$$

$$v_{20}=g_0(\xi,\tilde{t}) \tag{26}$$

where the two moving coordinates $\sigma\equiv x-2t/\Delta$, $\xi\equiv x-t/M$, were introduced, and $f_0(\sigma,0)=h_1(0)$, $g_0(\xi,0)=h_2(0)$.

To obtain the dependence on σ, ξ and $\tilde{t}$, the next order in the expansion is considered. After considerable algebra, one finds

$$\boldsymbol{\eta}_{1,t}+\boldsymbol{A}\cdot\boldsymbol{\eta}_{1,x}=-\boldsymbol{\eta}_{0,\tilde{t}}+\boldsymbol{C}\cdot[\eta_{10}\eta_{10,x},\eta_{20}\eta_{20,x}]^{\mathrm{T}}+(\eta_{10}\eta_{20})_x\boldsymbol{d}-\kappa^2\boldsymbol{e}_{xx}, \tag{27}$$

where

$$\boldsymbol{C}=\frac{2(M-1)}{M\Delta^2}\begin{bmatrix} M+1-(M-1)\lambda_2 & -(M-1)(\lambda_1-1) \\ -(1+\lambda_2)(M-1) & -(M+1+\lambda_1(M-1)) \end{bmatrix},$$

$$\boldsymbol{d}=\frac{(M-1)}{M\Delta^2}\begin{bmatrix} (M-1)(\lambda_1+\lambda_2)-2M \\ (M-1)(\lambda_1+\lambda_2)+2M \end{bmatrix},$$

and the vector $\boldsymbol{e}$ is a complicated expression involving $\phi_0, \eta_0, \ldots$ and their spatial derivatives (Zeybek 1991). Equivalently, we may use transform (22) to obtain

$$\boldsymbol{v}_{1,t}+\boldsymbol{D}\cdot\boldsymbol{v}_{1,x}=-\boldsymbol{v}_{0,\tilde{t}}-\boldsymbol{L}\cdot\boldsymbol{C}\cdot[\eta_{10}\,\eta_{10,x},\eta_{20}\,\eta_{20,x}]^{\mathrm{T}}-(\eta_{10}\,\eta_{20})_x\boldsymbol{L}\cdot\boldsymbol{d}+\kappa^2\boldsymbol{L}\cdot\boldsymbol{e}_{xx}. \quad (28)$$

Use of (23)–(26) into (28) leads after considerable algebra to

$$\left(\frac{2}{\Delta}-\frac{1}{M}\right)v_{11,\xi}=-v_{10,\tilde{t}}+\frac{4(M-1)}{\Delta^2}(2+\lambda_2-\lambda_1)\,v_{10}\,v_{10,\sigma}$$

$$+\frac{k^2(M-1)}{M\Delta}(a_{11}\,v_{10,\sigma\sigma\sigma}+a_{12}\,v_{20,\xi\xi\xi}) \quad (29)$$

and

$$-\left(\frac{2}{\Delta}-\frac{1}{M}\right)v_{12,\sigma}=-v_{20,\tilde{t}}+\left(\frac{M-1}{M\Delta}\right)(2+\lambda_2-\lambda_1)(v_{20}\,v_{10,\sigma}+v_{10}\,v_{20,\xi})$$

$$+\frac{\kappa^2(M-1)}{M\Delta}[a_{21}\,v_{10,\sigma\sigma\sigma}+a_{22}\,v_{20,\xi\xi\xi}]. \quad (30)$$

After integration of (29) with respect to ξ, all secular terms vanish if the terms containing v_{10} also vanish, thus ($U\equiv v_{10}$)

$$U_{\tilde{t}}=\frac{4(M-1)}{\Delta^2}(2+\lambda_2-\lambda_1)\,UU_{\sigma}+\frac{(M-1)\,\kappa^2}{M\Delta}a_{11}\,U_{\sigma\sigma\sigma}. \quad (31)$$

Similarly working for the other component in (30) and eliminating secular terms yields

$$V_{\tilde{t}}=\frac{(M-1)\,\kappa^2}{M\Delta}a_{22}\,V_{\xi\xi\xi}, \quad (32)$$

assuming sufficiently fast decay to zero. The two coefficients in (31) and (32) are given by

$$a_{11}=\frac{4M}{3\Delta}\frac{(\lambda_2-\lambda_1)(1+\lambda_2-\lambda_1)[(\lambda_2+1)^2+(\lambda_1-1)^2+(\lambda_2+1)(\lambda_1-1)]}{(2+\lambda_2-\lambda_1)},$$

$$a_{22}=\frac{(1-\lambda_1)(\lambda_1-\lambda_2)(1+\lambda_2)\Delta}{M(2+\lambda_2-\lambda_1)},$$

and they are related to $x_{2,1}$ and $x_{2,2}$ by $a_{ii}=M\Delta x_{2,i}/(M-1)\,(i=1,2)$. The various parameters in (31)–(32) are functions of the undisturbed interface positions λ_1,λ_2, and the mobility ratio M. For the full problem, the solution of both (31) and (32) is required. Note the following: (i) purely translational motion occurs when $M=1$, as expected; (ii) there are two long-wave speeds, $2/\Delta$ and $1/M$, both decreasing to zero as the viscosity ratio increases. The long-wave speed $1/M$ corresponding to variable V is simply the dimensionless (undisturbed) velocity of fluid b; (iii) as anticipated, the linearized equations yield the leading order of the linear analysis; (iv) the dispersive term in the KdV equation vanishes when $1+\lambda_2-\lambda_1=0$ (which, for the symmetric case $\lambda_1=-\lambda_2$, coincides with the Saffman–Taylor finger width $\lambda_1=\frac{1}{2}$); (v) antisymmetric disturbances ($\eta_1=\eta_2$) are governed by the Airy equation (32) alone; (vi) finally,

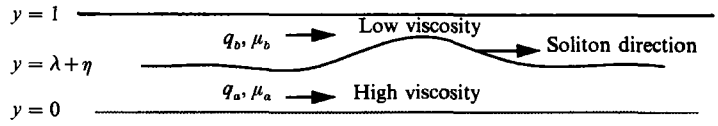

FIGURE 2. Counterflow of the two fluids in a moving frame of reference.

when both initial and disturbed interfaces are symmetric ($\lambda_1 = -\lambda_2$ and $\eta_1 = -\eta_2$), the interface motion is governed by the KdV equation alone. The latter is of great interest for the subsequent experiments. This case may be recast in terms of the original variables as follows ($\lambda \equiv \lambda_1$):

$$\eta_t + c_0 \eta_x - 2(M-1) c_0^2 \eta\eta_x + \tfrac{1}{3}\epsilon c_0^2 \kappa^2 (M-1)\lambda(1-2\lambda)(1-\lambda)\eta_{xxx} = 0. \tag{33}$$

Equation (33) can be interpreted as follows. Owing to parallel flow, any initial disturbance travels with a long wave speed c_0. The latter always lies between the velocities of the two fluids (e.g. $1 < c_0 < 1/M$ for $M < 1$). For an observer travelling with speed c_0 the fluid flow is counter-current, the lower-viscosity fluid flowing towards the right and the higher-viscosity fluid towards the left in the schematic of figure 2 (where one must recall that in the Hele-Shaw context, viscous shear is not relevant to long waves). Because of unequal viscosities, the long-wave disturbances also disperse, to the left if $(M-1)(1-2\lambda) > 0$, and to the right, otherwise. We note that shorter-wavelength dispersion, although possible, is likely to be damped by capillarity and wettability effects. Sustained wave propagation is possible only if amplitudes are small and the nonlinearity is weak. Strong nonlinear effects must be excluded. They violate parallel flow conditions and are likely to lead to frontal motion and viscous fingering. Nonetheless, weakly nonlinear waves also tend to break, to the left if $(M-1)\eta > 0$, and to the right, otherwise. For the positive disturbance of figure 2, dispersion will oppose breaking if $1-2\lambda < 0$. Under this condition, a permanent-form wave would develop, that propagates to the left or to the right, depending on whether $M > 1$ or $M < 1$, respectively. Analogous conclusions can be drawn for all other possibilities.

In the symmetric case we may use classical results (Drazin & Johnson 1989) to predict in advance the possibility of solitary waves, in terms of M, the interface position λ_1 and the initial shape of the disturbance. With the use of the rescaling

$$u \to \alpha\eta; \quad x \to \beta\sigma; \quad t \to t,$$

where

$$\beta = -[\tfrac{1}{3}\epsilon c_0^2 \kappa^2 (M-1)\lambda(1-2\lambda)(1-\lambda)]^{-\frac{1}{3}}, \quad \alpha = -\tfrac{1}{3}(M-1)c_0^2\beta,$$

equation (33) can be mapped into the standard form

$$u_t - 6uu_x + u_{xxx} = 0 \tag{34}$$

with initial condition

$$u(x,0) = -u_0 \operatorname{sech}^2(b(x-x_0)).$$

Then, the theory predicts the following. (i) When $\lambda_1 > 0.5$, $M < 1$, $\eta > 0$, and $\lambda_1 < 0.5$, $M > 1$, $\eta < 0$, solitons develop and propagate in the positive σ-direction. (ii) When $\lambda_1 > 0.5$, $M > 1$, $\eta > 0$, and $\lambda_1 < 0.5$, $M < 1$, $\eta < 0$, solitons propagate in

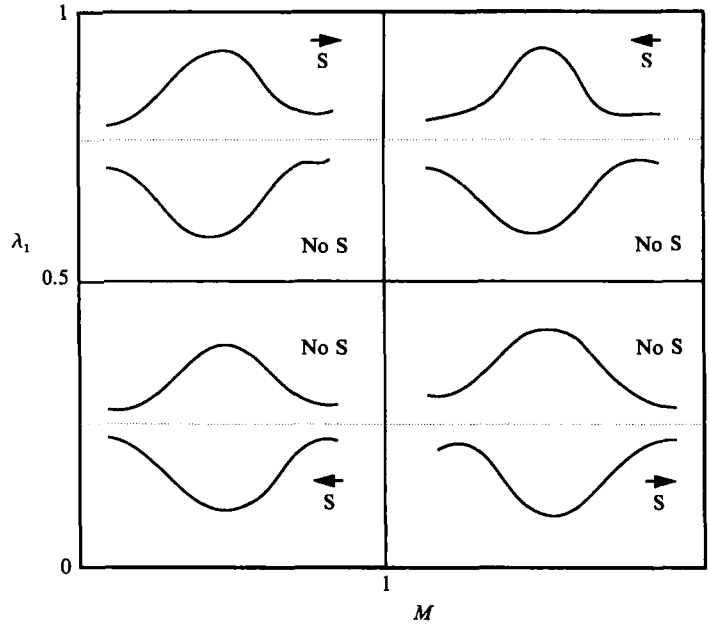

FIGURE 3. M *vs.* λ_1 diagram for formation of solitons (S).

the negative σ-direction. (iii) No solitons would form in any other case. Based on the above, the phase diagram of figure 3 can be constructed. Both the existence of solitons and their direction of propagation, in a frame of reference moving with speed $2/\Delta$, are shown. The map will be repeatedly used below in the comparison between experiment and theory.

2.3. *Numerical method*

Although we shall often use general exact results, we shall rely for illustration purposes on numerical results, obtained with the pseudospectral technique of Fornberg & Whitham (1978). The method combines a Fourier transform treatment of the space dependence with a leapfrog scheme for the time evolution and it is well suited for nonlinear dispersive waves. The interval l is discretized into N equidistant points, with spacing $\Delta x = l/N$ (N was taken as 128, 256 or 512). The function $\eta(x,t)$ is discrete Fourier-transformed with respect to x by the use of a fast Fourier transform algorithm. Thus (33) is discretized as follows:

$$\eta_i^{n+1} - \eta_i^{n-1} = -2\mathrm{i}\Delta t c_0 \mathscr{F}^{-1}\left[\frac{2\pi}{N} n \mathscr{F}(\eta)\right] + 2\mathrm{i}(2(M-1)c_0^2)(\eta_i^n)\,\Delta t \mathscr{F}^{-1}\left[\frac{2\pi}{N} n \mathscr{F}(\eta)\right]$$

$$-2\mathrm{i}(\tfrac{1}{3}\epsilon\kappa^2 c_0^2)(M-1)\lambda(1-2\lambda)(1-\lambda)\mathscr{F}^{-1}\left[\sin\left(\left(\frac{2\pi}{N}\right)^3 n^3 \Delta t\right)\mathscr{F}(\eta)\right]. \quad (35)$$

The numerical scheme was tested favourably with an exact soliton solution, as well as with the test example of Zabusky & Kruskal (1965). A similar discretization was implemented for the Airy equation.

In the experiments that follow, the existence of solitons was tested by direct comparison with simulation, but also by looking for the following key properties (Drazin & Johnson 1989): (i) arbitrary initial disturbances evolve into one or more solitons and into dispersive waves of substantially smaller amplitude; (ii) the speed

of a soliton depends on its amplitude, which increases with an increase in amplitude; (iii) solitons regain their identity after interaction with other solitons. For a given initial condition, the number of solitons and their amplitude can be predicted from the standard theory of the KdV equation (Drazin & Johnson 1989; Whitham 1974). For example, the number of solitons obeys the condition

$$N \leqslant \left[\left(\frac{u_0}{b^2}+\frac{1}{4}\right)^{\frac{1}{2}}-\frac{1}{2}\right]+1, \tag{36}$$

while the soliton amplitude is

$$a_n = 2\kappa_n^2, \tag{37}$$

where

$$\kappa_n = \tfrac{1}{2}b\left[\left(1+\frac{4u_0}{b^2}\right)^{\frac{1}{2}}-(2n-1)\right]. \tag{38}$$

These were used in the subsequent comparison with the experiments.

3. Experimental

As in shallow water wave experiments, the two small parameters δ and ϵ play a critical role. The conditions $\delta, \epsilon \ll 1$ suggest that a satisfactory resolution (larger A) requires larger cell width, which in turn requires proportionally larger length. Therefore, the construction of a narrow and long Hele-Shaw cell was necessary in order to observe possible solitary waves (Maxworthy 1987; Park, Gorell & Homsy 1984; Saffman & Taylor 1958; Tabeling, Zocchi & Libchaber 1987). The cell consisted of two Plexiglas plates, $\frac{1}{2}$ in. thick, of dimensions 230×27 cm, and of a rubber gasket spacer 0.08 cm thick. Since interferometric methods (Tabeling *et al.* 1987) were not available, the uniformity of the gap was estimated by the indirect method of Park *et al.* (1984). The linear regression coefficient of the data was 0.999, indicating a good uniformity of the cell. The plates were held together using C-clamps. The experimental set-up consists of the Hele-Shaw cell in a horizontal position, three integral variable-speed peristaltic pumps, a video camera, a video recorder and a monitor (see figure 4). The frame of the cell was constructed such that it could be tilted with respect to both the transverse and the longitudinal axes. This was necessary in order to establish the steady-state interfaces.

Experiments reported below were conducted with two different fluid pairs. The first pair is mineral oil and glycerol/water solution with corresponding viscosities 170 cP and 860 cP, while the second pair is DC 200 silicon fluid and glycerol/water solution with corresponding viscosities 1060 cP and 500 cP. Mineral oil is the wetting fluid in the first pair, while DC 200 silicone fluid is the wetting fluid in the second pair. The viscosities of the fluids were measured by both a Cannon-Fenske and a Brookfield spindle viscometer. Since the parallel flow condition is one on fluid viscosities ($q_a \mu_a = q_b \mu_b$), the accuracy of these measurements plays an important role in establishing the flat interface. Relatively high flow rates were used, such that the modified capillary number was typically $O(10^2)$. No sustained wave propagation was observed for substantially lower N'_{ca} values. This is consistent with the theory. The experiments were conducted with configurations involving both one and two interfaces. The single-interface case corresponds to the symmetric case ($\lambda_1 = -\lambda_2$, $\eta_1 = -\eta_2$). This configuration can be viewed either as the top or the bottom half of the symmetric problem. It can be easily checked that the solution of (33) is invariant to the change $\lambda_1 \to 1+\lambda_2$, $\eta_1 \to \eta_2$, $M \to 1/M$ (please note also the rescaling of time), thus

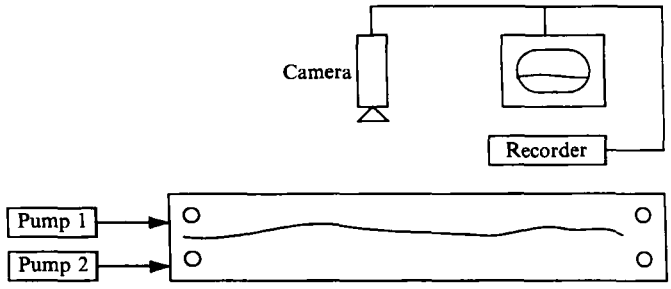

FIGURE 4. Experimental set-up.

without loss we may view the flow as the top half of a symmetric problem with the 'lower' fluid being fluid a. In our experiments, this was the more viscous fluid for the case $M = 0.2$ and the less viscous fluid for the case $M = 2.1$.

Conducting the flow experiments consists of two stages. The first stage is to establish a flat lateral fluid interface and parallel flow conditions for the two fluids. For the single-interface case, this is accomplished by a displacement process with the aid of gravity. The cell is first filled with one fluid. While the cell is tilted on its side, the lighter fluid is slowly injected at the top. Subsequently, the cell is slowly returned to horizontal position. The parameter λ, which is the dimensionless location of the interface, is controlled by the relative amounts of fluids injected. For the non-symmetric case, flat interfaces are established by the simultaneous injection of both fluids, while the cell is slightly tilted on the transverse axis. We were unable to independently vary the locations of both top (λ_1) and bottom (λ_2) interfaces, which shifted together according to the amounts of the fluids injected. We stress that in the two-interface problem, the parallel flow condition, $\mu_b q_b = \mu_a q_a$, was found essential for the establishment of a parallel interface. Under conditions such that the modified capillary number is relatively large, flat interfaces were obtained with an accuracy of ± 1 mm.

The second stage is to introduce a disturbance as an initial condition, typically obtained by interrupting momentarily the flow of one fluid, and to monitor the motion of the disturbance. The wavelength and amplitude of the disturbances were controlled by the speed of the interruption. Although results obtained with such initial conditions were generally satisfactory, questions may arise as to the effect of flow interruption and end effects. This will be discussed in a later section.

4. Results and discussion

4.1. *Symmetric case*

Three different cases were considered corresponding to three different viscosity ratio regimes ($M < 1, M \sim 1, M > 1$).

4.1.1. $M < 1$

Here, the first pair of fluids (mineral oil and water/glycerol solution) was used with $M = 0.2$. Figure 5 shows typical experimental results in digitized pictures taken from a videotape. A hump-like initial disturbance taken to satisfy the small-amplitude and long-wave conditions was imposed on the parallel interface ($\lambda = 0.69$) (figure 5a). The cell width here is 6 cm. For the particular initial conditions of wavelength $L = 20$ cm, and amplitude 1 cm, the theory predicts a single soliton travelling

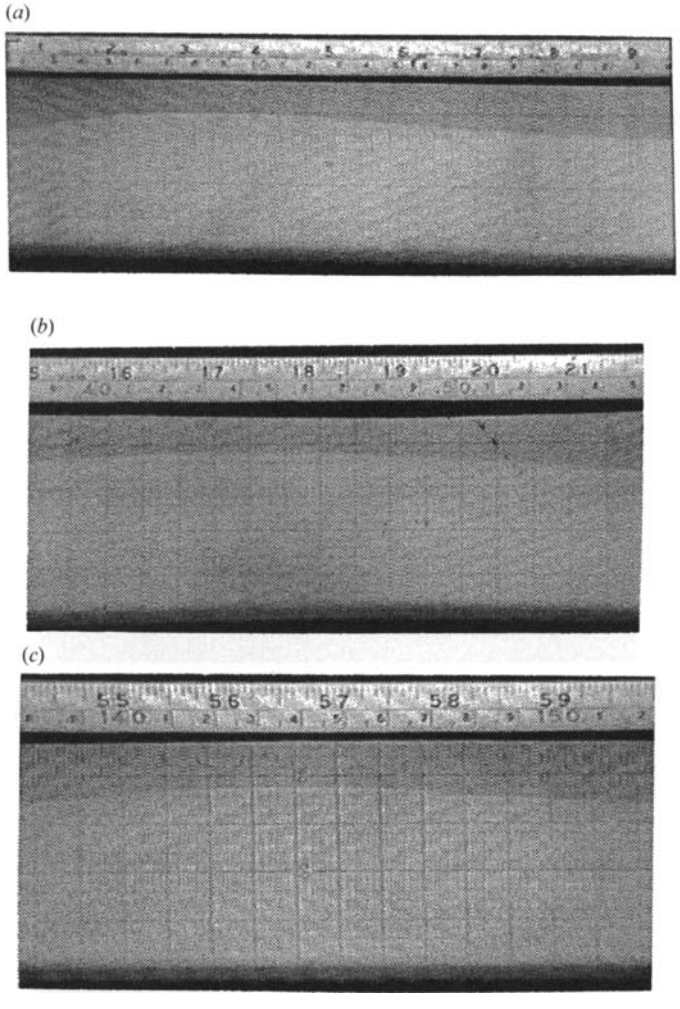

FIGURE 5. Single solitary wave: (*a*) initial condition, (*b*, *c*) subsequent stages.

forward ($\lambda > \frac{1}{2}, M < 1, \eta > 0$) (see figure 3). Indeed, upon restoration of the flow rate to the initial level, the disturbance was advected by the flow, and it started developing into a wave of constant shape followed by a wiggly interface of small amplitude and short wavelength behind it. Typically, this constant-amplitude wave has taken a permanent form after travelling about 45 cm, and appeared to possess all the characteristics of a soliton (figure 5*b*). The amplitude is clearly different from the initial one and remains constant for a substantial distance travelled (figure 5*c*), as long as 150 cm, beyond which end effects seem to become appreciable. Numerical simulations corresponding to these conditions and for the initial shape of figure 5(*a*) are shown in figure 6.

The comparison between theory and experiment shows a quite satisfactory agreement, despite the ambiguity on the suitability of the initial condition for the experiment (recall that the disturbance is imposed by flow interruption). The theoretical and experimental number of solitons coincide (equal to 1), while computed and observed final amplitudes were 0.81 cm and 0.76 cm, respectively. The wave velocity with respect to a fixed observer was calculated to be 0.28 cm/s, which

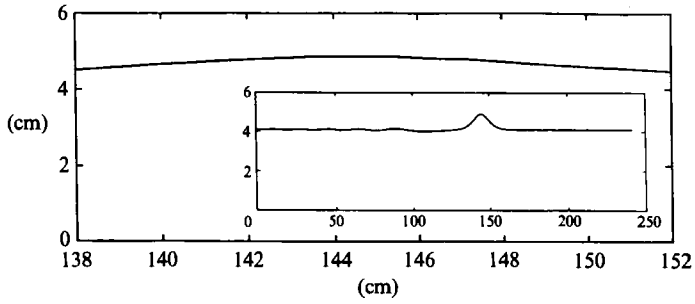

FIGURE 6. Numerical simulation of figure 5(*c*). Inset: profile in different scales.

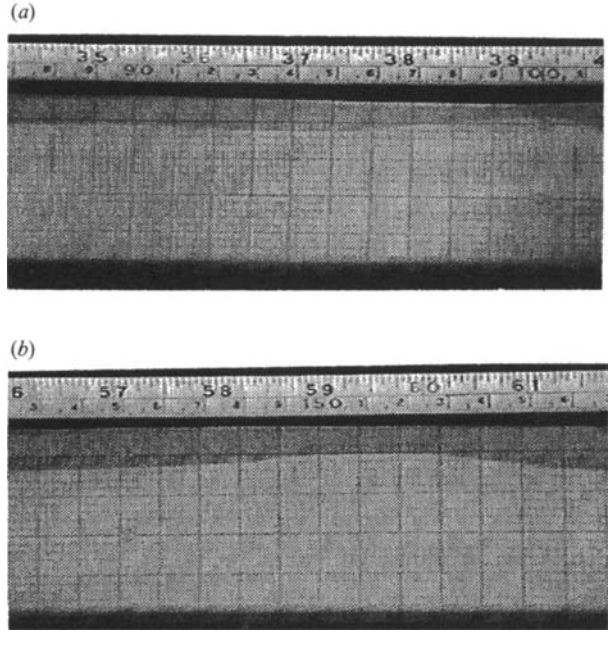

FIGURE 7. Two solitary waves at two different stages.

compares well with the experimental value of 0.26 cm/s. Owing to the particular scales selected to match one-to-one the experimental pictures, certain typical characteristic features of soliton and dispersive waves are suppressed in figure 6. To illustrate this point, the profile of figure 6 is replotted in the inset with different scales. Nonetheless, motion of dispersive waves was actually not observed to our satisfaction in the experiments. Typically, a noisy and wiggly interface of small wavelength and amplitude formed soon after the main wave evolved. However, we suspect that wettability and surface tension have likely played major roles on its subsequent development.

Figure 7 shows the emergence of two solitons arising from an initial disturbance of longer wavelength ($L \sim 45$ cm). According to the theoretical predictions, two solitary waves of different amplitudes (and speed) should arise, in order of descending amplitudes (figure 7). As time progresses, the two solitons are clearly separated, the higher-amplitude soliton moving faster and away from the trailing lower-amplitude soliton. Figure 7(*b*) is a picture of the trailing wave. A typical characteristic of the emergence of more than one soliton is an increase in the amplitude after the onset of

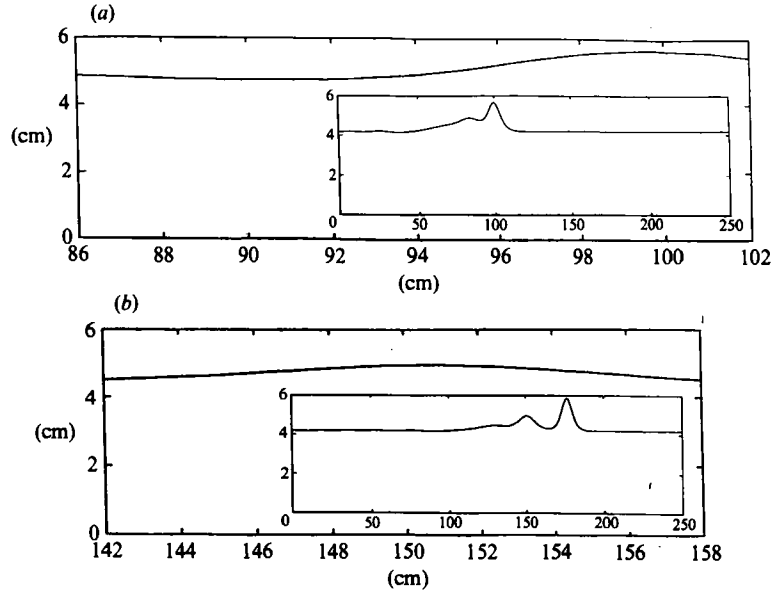

FIGURE 8. Numerical simulation of figure 7. Inset: profile in different scales.

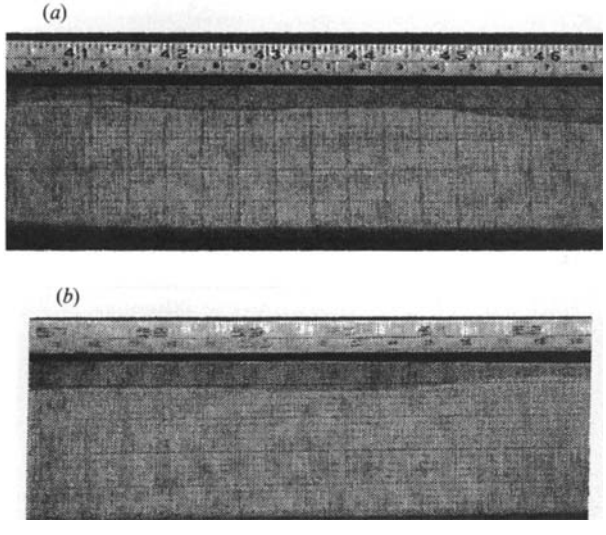

FIGURE 9. Two solitary waves, (*a*) before and (*b*) after interaction.

the initial disturbance. This feature was clearly observed. Comparison with the numerical simulations is again quite satisfactory (see figure 8 and the inset with different scales).

Under the same conditions, soliton interaction is shown in figure 9. To create the two solitary waves, two disturbances of different amplitude were sequentially introduced. The second disturbance is of higher initial amplitude and evolves into a faster soliton that eventually takes over the preceding slower one. After this nonlinear interaction, tall and short solitons reappear, but in reverse order and propagate with their original speed (figure 9*b*). All these features are consistent with the theory. Corresponding numerical simulations are in good agreement as shown in

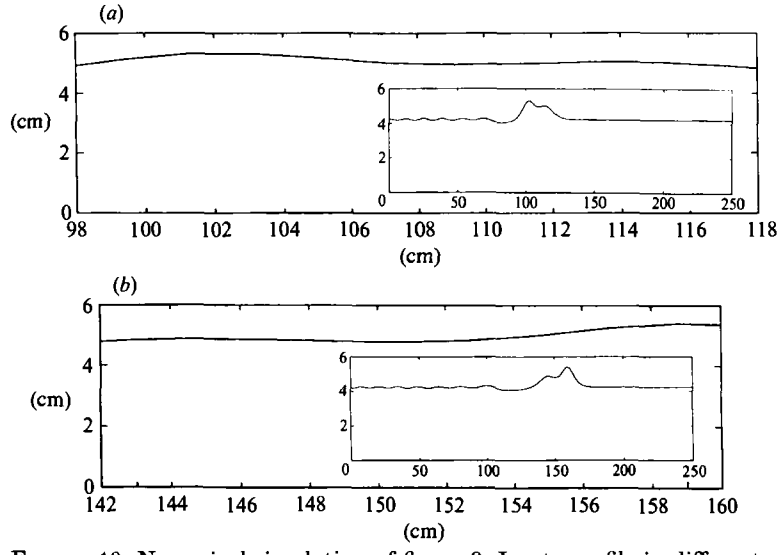

FIGURE 10. Numerical simulation of figure 9. Inset: profile in different scales.

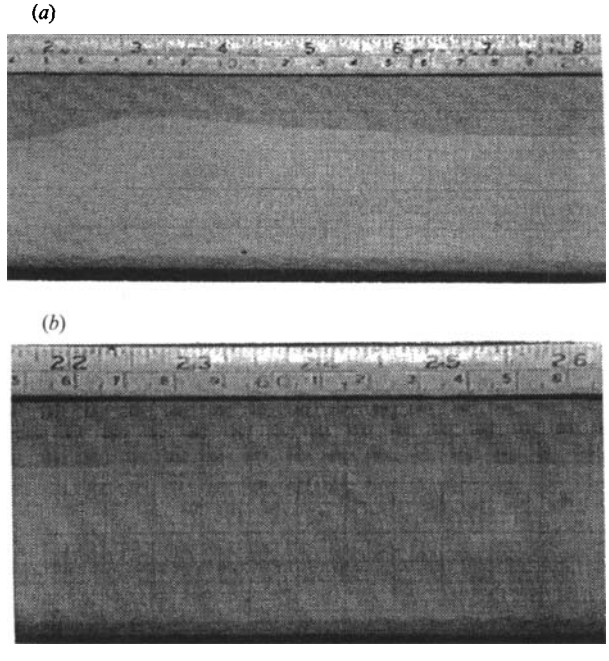

FIGURE 11. (a) Short-wave initial disturbance and (b) subsequent stage.

figure 10. Some additional effects were also considered. For instance, short-wave disturbances, typically corresponding to $\delta \geqslant 0.5$, were found to dissipate after their onset, as predicted by the theory. Figure 11 shows such a short-wave disturbance and its subsequent stage, where the amplitude has significantly decreased over a rather short distance. Numerical simulations are also in agreement.

For disturbances in the opposite negative direction ($\eta < 0$), no solitons are predicted by the theory (compare figure 3). This prediction was tested in the experiments. Consistent with the theory, any such disturbances (whether of long or

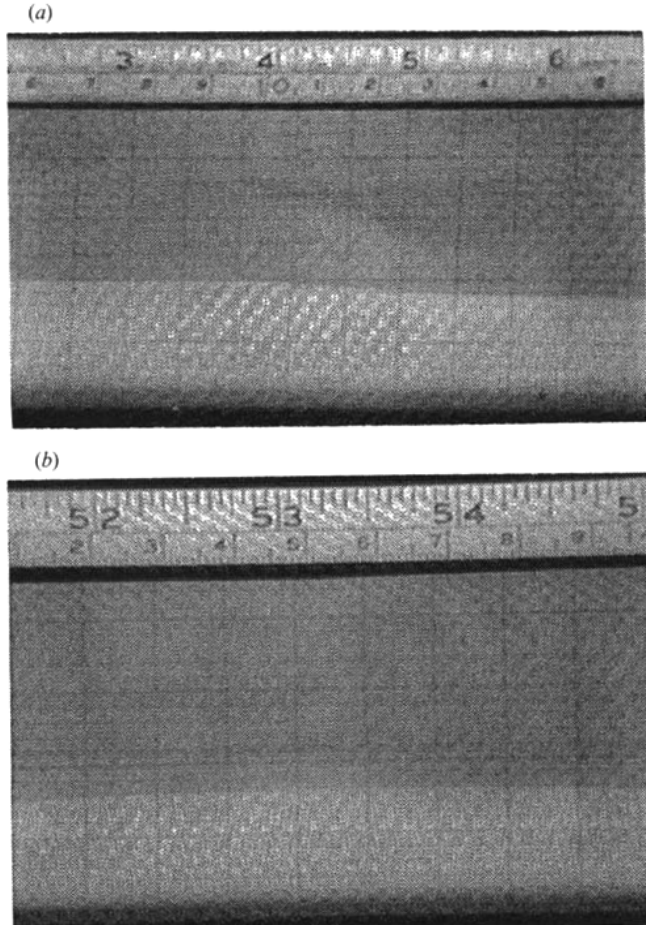

FIGURE 12. Experiment with $\lambda < \frac{1}{2}$ and positive initial disturbance.

short wavelength) dissipated continuously, although it is quite likely that wettability may have also interfered with the interface dynamics in this case (see below). Similarly, for $0 < \lambda < \frac{1}{2}$, but with a positive initial disturbance, no solitons are theoretically predicted. A typical experimental run for such conditions ($\lambda = 0.3$) is shown in figure 12. The corresponding simulation result was also in good agreement with the experiment. Finally, when $0 < \lambda < \frac{1}{2}$, and the initial disturbance is negative, solitons are predicted to propagate in the negative σ-direction (figure 3). Unfortunately, this disturbance could not be introduced clearly and solitons were not observed, although dispersive-like waves travelling ahead of the main disturbance were noticed and the advective velocity agreed with the theory to some degree. We believe that the reason for this discrepancy is wettability. Indeed, soliton propagation in the negative σ-direction (which is equivalent to this case) was observed when we experimented with a different pair of fluids of different viscosity ratio ($M > 1$), but with reverse wettability.

4.1.2. $M \sim 1$

The second region of interest in figure 3 corresponds to equal-viscosity fluids. Experiments were carried out with a pair of mineral oil and water/glycerol solution of nearly equal viscosity ($M = 0.97$). In this case, both the nonlinear and the

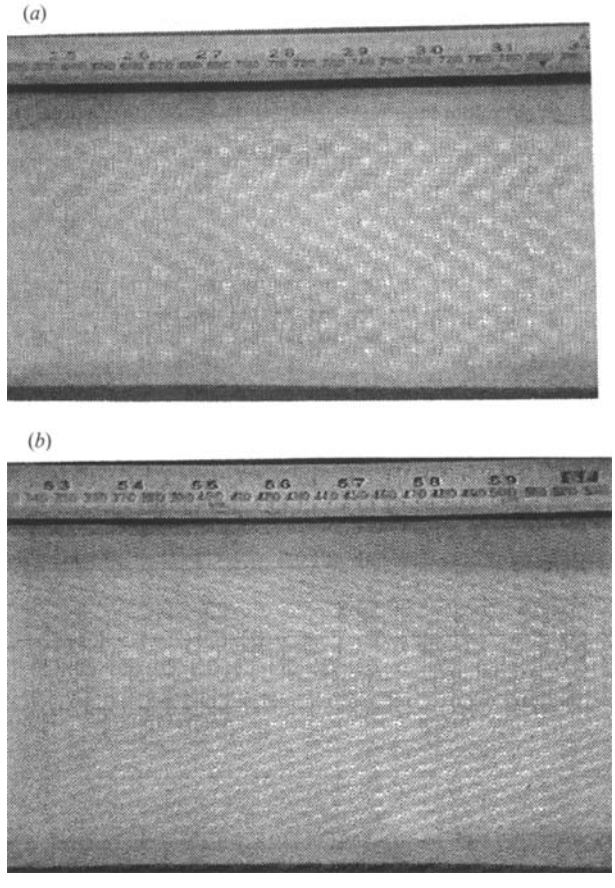

FIGURE 13. The non-symmetric case: single soliton at two different stages.

dispersive terms in the KdV equation (33) are very small, hence we expect constant wave speed and translational motion independent of the wave amplitude. In the experiments, disturbances similar to figure 5 were introduced. However, neither a change in shape nor a wiggly interface were observed. The disturbance simply propagated with a constant speed, equal to the fluid velocities (Zeybek 1991). As a second test, two disturbances with different amplitudes were sequentially introduced, in a way analogous to the soliton interaction case discussed above. It was observed that the distance between the two disturbances remained constant and that no further interaction occurred. This behaviour is fully consistent with the theory.

4.1.3. $M > 1$

Finally, for completeness, we also considered the case with $M > 1$. As pointed out above, this case is symmetric to $M < 1$, thus results identical to the previous should be obtained under the appropriate conditions. The condition $M > 1$ required a different pair of fluids; however, the wettability was not altered (the top fluid was still wetting the surface). We used DC 200 silicon fluid and glycerol/water solution with $M = 2.1$. Solitons are predicted to move to the left on the σ-axis for $M > 1$, $\lambda > \frac{1}{2}$ and $\eta > 0$ (figure 3).

The first experiment was to generate a single soliton. As in the previous case, it was

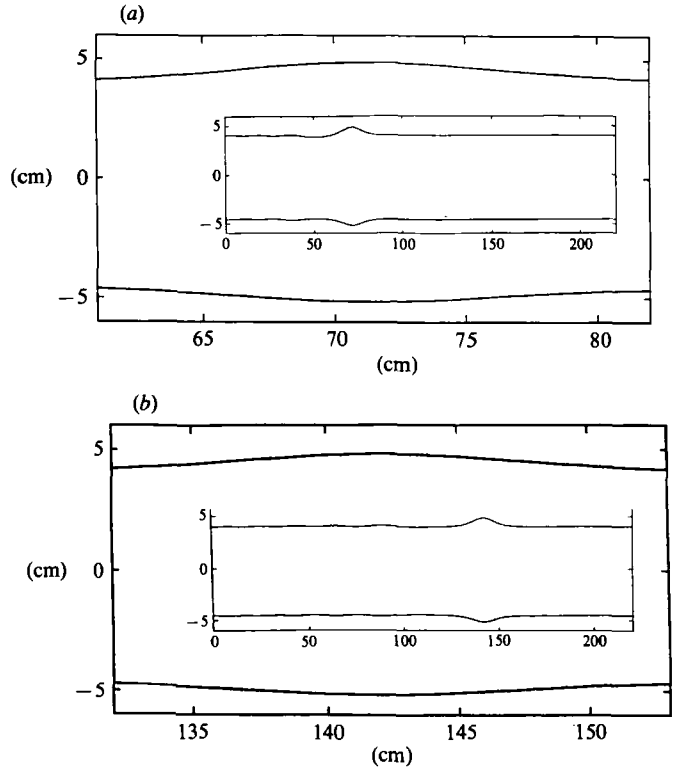

FIGURE 14. Numerical simulation of figure 13.

satisfactory (Zeybek 1991). Interaction of solitons was sought in a subsequent experiment. Contrary to the case $M < 1$, we first introduced the higher-amplitude disturbance, which evolves into a higher-amplitude soliton, to be followed by the lower-amplitude disturbance, which evolves into a lower-amplitude soliton. According to the theory, for a fixed observer, the lower-amplitude soliton travels faster and eventually overtakes the higher-amplitude soliton. This was clearly observed. Because of limitations on the length of the cell, however, complete reappearance of the lower-amplitude soliton after the interaction was not possible. As before, the experimental run and the corresponding numerical simulation were in good agreement (Zeybek 1991).

4.2. *Non-symmetric case*

Although the experiments in the symmetric case appear to support the theory, we also experimented with the non-symmetric configurations. Two different channel widths ($2W = 9$ and 12 cm) were used. As in the first set of experiments, the pair of fluids consisted of mineral oil (outer fluid) and glycerol/water solution (inner fluid). The flat lateral interfaces were established by the simultaneous injection of the two fluids.

In the experiments below, we used $\lambda_1 = 0.65$ and $\lambda_2 = -0.76$. Two disturbances, of initial amplitude 1.2 and -0.75 cm, respectively, were simultaneously generated on each interface. Figure 13 shows the solitary waves that developed on each interface. The two waves retained their shapes even after they have travelled a distance of about 140 cm. Wiggly interfaces suggesting dispersive waves were

observed in the back of the waves. Figure 14 shows the corresponding numerical simulations.

Interaction of solitons was also studied. Here, two different-amplitude disturbances were sequentially introduced on each interface. Numerical simulations confirmed the experimental findings. Other conditions were also tested for different values of λ_1 and λ_2. In the non-symmetric case, the value of the parameter $\lambda_1 - \lambda_2$ is critical. When $\lambda_1 - \lambda_2 < 1$ (interfaces are closer to each other), all other conditions remaining the same, the disturbances dissipated. For additional details, Zeybek (1991) should be consulted. Unfortunately, the experimental amplitudes were too small for satisfactory identification and comparison. Further work on this and related issues is currently underway.

5. Concluding remarks

The small-amplitude long-wave motion of lateral interfaces in parallel flow was investigated at large values of N'_{ca} in a long, horizontal Hele-Shaw cell. The asymptotic theory for the case of two fluids was formulated in terms of a set of KdV and Airy equations. The findings of the theory were validated by experiments involving both one (symmetric case) and two interfaces (non-symmetric case). Under the condition $\mu_b q_b = \mu_a q_a$, flat interfaces pertaining to parallel flow were successfully established in each case. Experimental results supported, for the most part, the theoretical predictions including the existence of solitons. It is important to point out that this is the first time that Hele-Shaw (and, perhaps porous media) flows have been reported to contain KdV dynamics (although see also Kadanoff (1990) *in a* different context). However, some experimental aspects still remain unclear.

Dispersive waves associated with solitons should appear in the experiments. These waves can be identified in the simulations, although only at a high resolution. However, they were not observed in the experiments. A wiggly shape did develop at the points where it was supposed to be present. This was observed in both forward and backward moving solitons. We believe that it is indeed the initial motion of the dispersive waves that initiates these noisy interfaces. However, the subsequent motion is largely controlled by surface tension and wettability effects which become important at small wavelengths. Significantly, no wiggly interface was observed in the experiments with equal-viscosity fluids ($M \sim 1$).

Along the same lines, it was pointed out that the direction of the initial disturbance was critical to the development of wave motion. In all cases, the experiments were successful when the initial disturbance was in the direction of drainage (non-wetting displacing wetting). The results of experiments were inconclusive when the disturbance was introduced in the opposite (imbibition) direction, when it was observed that the shape of disturbance was not as well defined as in the drainage case. We demonstrated this for the simplest case of equal viscosities, $M \sim 1$. Quite satisfactory results were obtained when the disturbance was positive (from non-wetting to wetting). Results much different than expected, and generally not in agreement with the theory, were obtained when the disturbance was in the opposite direction (from wetting to non-wetting fluid). Wettability and related effects are certainly in need of further investigation.

Finally, in some cases the velocity of the frame of reference was quite large compared to the soliton speed, thus we were not able to monitor the full extent of the wave motion. With the aid of gravity, this velocity of the frame of reference can be reduced to zero. However, now the flow directions must be opposite to each other.

Such experiments are currently underway. Parallel theoretical developments involving waves in the presence of gravity in Hele-Shaw flows are reported in Meiburg (1991).

This work was supported in part by DOE contract DE-FG22-90BC14600, the contribution of which is gratefully acknowledged. Acknowledgment is also made to the donors of The Petroleum Research Fund, administered by the ACS, for partial support of this research.

REFERENCES

ABLOWITZ, M. J. & SEGUR, H. 1981 *Solitons and the Inverse Scattering Transforms*. SIAM.

AUL, R. W. & OLBRICHT, W. L. 1990 Stability of a thin annular film in pressure driven low Reynolds number flow through capillary. *J. Fluid Mech.* **215**, 585–599.

BENSIMON, D., KADANOFF, L. P., LIANG, S., SHRAIMAN, B. I. & TANG, C. 1986 Viscous flows in two dimensions. *Rev. Mod. Phys.* **58**, 977.

BURGESS, D. & FOSTER, M. R. 1990 Analysis of the boundary conditions for a Hele-Shaw bubble. *Phys. Fluids* **2**, 1105–1117.

COATS, K. R., DEMPSEY, J. R. & ANDERSON, J. H. 1971 The use of vertical equilibrium in two dimensional simulation of three dimensional reservoir performance. *Soc. Petrol. Engrs J.* **11**, 63–71.

COLLINS, R. E. 1967 *Flow of Fluids Through Porous Media*. Tulsa: Petroleum Publishing Co.

COMBESCOT, R., DOMBRE, T., HAKIM, V., POMEAU, Y. & PUMIR, A. 1986 Shape selection of Saffman–Taylor finger. *Phys. Rev. Lett.* **56**, 2036–2039.

DRAZIN, P. G. & JOHNSON, R. J. 1989 *Solitons: An Introduction*. Cambridge University Press.

EMANUEL, A. S., ALAMEDA, G. K., BEHRENS, R. A. & HEWETT, T. A. 1989 Reservoir performance prediction methods based on fractal geostatistics. *Soc. Petrol. Engrs Reservoir Engng* **4**, 311–318.

FAYERS, F. J. 1988 An approximate model with physically interpretable parameters for representing miscible viscous fingering. *Soc. Petrol. Engrs Reservoir Engng* **3**, 551–558.

FAYERS, F. J. & NEWLEY, T. M. J. 1988 Detailed validation of an empirical model for viscous fingering with gravity effects. *Soc. Petrol. Engrs Reservoir Engng* **3**, 542–551.

FORNBERG, B. & WHITHAM, G. B. 1978 A numerical and theoretical study of certain nonlinear wave phenomena. *Proc. R. Soc. Lond.* A **289**, 373–403.

HAMMACK, J., SCHEFFNER, N. & SEGUR, H. 1989 Two-dimensional periodic waves in shallow water. *J. Fluid Mech.* **209**, 567–589.

HOMSY, G. M. 1987 Viscous fingering in porous media. *Ann. Rev. Fluid Mech.* **19**, 271–311.

KADANOFF, L. P. 1990 Exact solutions for the Saffman–Taylor problem with surface tension. *Phys. Rev. Lett.* **65**, 2986–2988.

KALAYDJIAN, F. & LEGAIT, B. 1987 Écoulement lent à contre-courant en imbibition spontanée de deux fluides non miscibles dans capillaire présentant un rétrécissement. *C.R. Acad. Sci. Paris* **304**, 869–875.

KEVORKIAN, J. & COLE, J. D. 1980 *Perturbation Methods in Applied Mathematics*. Springer.

KING, M. J. & SCHER, H. 1990 Geometric dispersion and unstable flow. *Phys. Rev.* A **41**, 874–883.

KING, P. R. 1987 The fractal nature of viscous fingering in porous media. *J. Phys., Paris* **20**, L529–L534.

LEE, J., CONIGLIO, A. & STANLEY, H. E. 1990 Fractal-to-nonfractal crossover for viscous fingers. *Phys. Rev.* A **41**, 4589–4592.

LENORMAND, R. 1989 Flow through porous media: limits of fractal patterns. *Proc. R. Soc. Lond.* A **423**, 159–168.

LENORMAND, R., KALAYDJIAN, F., BIEBER, M. T. & LOMBARD, J. M. 1990 Use of a multifractal approach for multiphase flow in heterogeneous porous media: comparison with CT-scanning experiment. Paper SPE20475 presented at the 65th SPE Annual Conference, New Orleans, LA, 22–26 Sept.

LENORMAND, R., TOUBOUL, E. & ZARCONE, C. 1988 Numerical models and experiments on immiscible displacements in porous media. *J. Fluid Mech.* **189**, 165–187.

LIGHTHILL, J. 1978 *Waves in Fluids.* Cambridge University Press.

MAXWORTHY, T. 1987 The nonlinear growth of a gravitationally unstable interface in a Hele-Shaw cell. *J. Fluid Mech.* **177**, 207–232.

MAXWORTHY, T. 1989 Experimental study of interface stability in a Hele-Shaw cell. *Phys. Rev.* A **39**, 5863–5866.

MEIBURG, E. 1991 Stability of rising air-bubbles in a Hele-Shaw cell. Maxworthy, T. **1991** Appendix to: The stability of inclined interfaces in a Hele-Shaw cell. *Phys. Fluids* A (submitted).

PARK, C. W., GORELL S. & HOMSY, G. M. 1984 Two phase displacement in Hele-Shaw cells: experiments on viscously driven instabilities. *J. Fluid Mech.* **141**, 257–287.

PARK, C. W. & HOMSY, G. M. 1984 Two-phase displacement in Hele-Shaw cells: theory. *J. Fluid Mech.* **139**, 291–308.

PELCÉ, P. 1988 *Dynamics of Curved Fronts.* Academic.

ROTHMAN, D. H. 1990 Macroscopic laws for immiscible two phase flow in porous media: results from numerical experiments. *J. Geophys. Res.* B **95**, 8663–8674.

SAFFMAN, P. G. & TAYLOR, G. I. 1958 The penetration of a fluid into porous medium or Hele-Shaw cell containing a more viscous liquid. *Proc. R. Soc. Lond.* A **245**, 312–329.

TABELING, P., ZOCCHI, G. & LIBCHABER, A. 1987 An experimental study of Saffman–Taylor instability. *J. Fluid Mech.* **177**, 67–82.

WHITHAM, G. B. 1974 *Linear and Nonlinear Waves.* John Wiley.

WITTEN, T. A. & SANDERS, L. M. 1981 Diffusion-Limited-Aggregation, a kinetic critical phenomenon. *Phys. Rev. Lett.* **47**, 1400–1403.

XU, J. J. 1991 Global instability of viscous fingering in a Hele-Shaw cell: formation of oscillatory fingers. Paper presented at the 44th Annual APS Meeting, Tampa, AZ, 24–26 Nov.

YOKOYAMA, Y. & LAKE, L. W. 1981 The effects of capillary pressure on immiscible displacements in stratified porous media. Paper SPE 10109 presented at the 56th Annual SPE Conference, San Antonio, TX, 5–7 Oct.

YORTSOS, Y. C. 1990 Instabilities in displacement processes in porous media. *J. Phys.: Condens. Matter* **2**, SA443–SA448.

YORTSOS, Y. C. & ZEYBEK, M. 1989 Long waves on Hele-Shaw fingers. Paper presented at the 1989 AIChE Fall Meeting, San Francisco, CA, 5–10 Nov.

ZABUSKY, N. J. & KRUSKAL, M. D. 1965 Interaction of solitons in a collisionless plasma and the recurrence of initial states. *Phys. Rev. Lett.* **15**, 240–243.

ZAPATA, V. J. & LAKE, L. W. 1981 A theoretical analysis of viscous crossflow. Paper SPE 10111 presented at the 56th Annual SPE Conference, San Antonio, TX, 5–7 Oct.

ZEL'DOVITCH, Y. B., ISTRATOV, A. G., KIDIN, N. I. & LIBROVICH, V. B. 1980 Flame propagation in tubes: Hydrodynamics and stability. *Combust. Sci. Tech.* **24**, 1–13.

ZEYBEK, M. 1991 Two studies in porous medial flows: long waves in parallel flow and dispersion effects on viscous instabilities. PhD thesis, University of Southern California.

ZEYBEK, M. & YORTSOS, Y. C. 1991 Long waves in parallel flow in Hele-Shaw cells. *Phys. Rev. Lett.* **67**, 1430–1433.